



HAL
open science

Intermittency in phytoplankton bloom triggered by modulations in vertical stability

Madhavan Girijakumari Keerthi, Marina Lévy, Olivier Aumont

► **To cite this version:**

Madhavan Girijakumari Keerthi, Marina Lévy, Olivier Aumont. Intermittency in phytoplankton bloom triggered by modulations in vertical stability. *Scientific Reports*, 2021, 11, pp.1285. 10.1038/s41598-020-80331-z . hal-03082241

HAL Id: hal-03082241

<https://hal.science/hal-03082241>

Submitted on 18 Dec 2020

HAL is a multi-disciplinary open access archive for the deposit and dissemination of scientific research documents, whether they are published or not. The documents may come from teaching and research institutions in France or abroad, or from public or private research centers.

L'archive ouverte pluridisciplinaire **HAL**, est destinée au dépôt et à la diffusion de documents scientifiques de niveau recherche, publiés ou non, émanant des établissements d'enseignement et de recherche français ou étrangers, des laboratoires publics ou privés.

Intermittency in phytoplankton bloom triggered by modulations in vertical stability

M. G. Keerthi^{1*}, M. Levy¹, and O. Aumont¹

¹ Sorbonne Université (CNRS/IRD/MNHN), LOCEAN-IPSL, Paris, France

***Corresponding author: Keerthi M G (keerthi.madhavan-girijakumari@locean.ipsl.fr)**

1 **Abstract**

2

3 Seasonal surface chlorophyll (SChl) blooms are very chaotic in nature, but traditional bloom
4 paradigms have climbed out of these subseasonal variations. Here we highlight the leading order
5 role of wind bursts, by conjoining two decades of satellite SChl with atmospheric reanalysis in
6 the Northwestern Mediterranean Sea. We demonstrate that weekly SChl fluctuations are in phase
7 with weekly changes in wind stress and net heat flux during the initial state of the bloom in winter
8 and early spring, thus expanding the convection shutdown hypothesis of bloom onset to
9 subseasonal timescales. We postulate that the mechanism reflected by this link is intermittency in
10 vertical stability due to short-term episodes of calm weather in winter or to stormy conditions in
11 early spring, leading to short-term variations in light exposure or to events of vertical dilution.
12 This strong intermittency in phytoplankton bloom may probably have important consequences
13 on carbon export and trophic web structure and should not be overlooked.

14

15

16

17 **Introduction**

18

19 A striking characteristic of phytoplankton blooms are the fluctuating patterns in sea-
20 surface Chlorophyll (SChl, a proxy for phytoplankton biomass) that punctuate the transition from
21 low abundance in winter to biomass accumulation in spring¹⁻¹⁰. The chaotic nature and varying
22 intensity of these subseasonal events make each seasonal cycle unique. In some years, the
23 temporal evolution of SChl deviates from the traditional pattern characterized by a single
24 seasonal peak and exhibits a succession of several peaks⁸. These subseasonal events make an
25 important contribution to bloom variability⁸ and are therefore an important factor for the
26 development of the upper trophic levels of the food web¹⁹ as well as for the efficiency of the
27 biological carbon pump²⁰.

28

29 Traditional bloom onset paradigms have climbed out of these subseasonal variations by
30 focusing on the strongest, or latest, peak. They relate the period of rapid growth of SChl between
31 winter and spring to the change in vertical stability, and to the increased light exposure of the
32 phytoplankton population associated with it. Under these models, a sustained bloom cannot start
33 before a seasonal tipping point is met, such as a critical depth or critical mixing intensity¹⁰⁻¹⁸.
34 This view is in conflict with the strong chaotic intermittency seen in SChl time series.
35 Incidentally, evidences of intermittent near-surface phytoplankton accumulation during spells of
36 calm weather in winter, with biomass being mixed down in the next storm, leading to a decrease
37 in SChl until weather conditions improve again, were present in the data sets used to test spring
38 bloom models^{11,12} but have been overlooked.

39

40 Here we explore the links between the surface bloom and vertical stability at
41 intraseasonal timescales, using two decades of satellite SChl data and atmospheric reanalysis in
42 the Northwestern Mediterranean Sea. Our focus on this region is motivated by a previous study
43 that highlighted the strong intensity of subseasonal SChl fluctuations there⁸. At the seasonal time
44 scale, Ferrari et al.¹¹ showed that surface blooms in the North Atlantic were triggered by a
45 change from cooling to heating in Net Heat Flux (NHF) at the end of winter, with a similar
46 dataset. They argued that this change resulted in a rapid shutdown of vertical convection. The
47 physical basis came from a preliminary numerical study which demonstrated that the reduction

48 in air-sea fluxes at the end of winter could be used as an indicator of reduced turbulent mixing¹⁰.
49 Our intention is to generalize this concept to all time scales from seasonal to subseasonal.
50 Intermittency in turbulent mixing being primarily driven by intermittency in atmospheric forcing,
51 we want to test whether subseasonal changes in SChl can be explained by subseasonal changes
52 in atmospheric conditions.

53
54 The seasonal phenology of SChl in the Northwestern Mediterranean Sea is well
55 documented²¹. As in the North Atlantic, it has been traditionally related to changes in the mixed-
56 layer depth (MLD)^{22,23}, with the SChl bloom starting as soon as the water column is more stable,
57 and a time lag of about one month between the time of maximum MLD in winter and maximum
58 SChl in spring. As a first step, we verified that the convection shutdown hypothesis of seasonal
59 bloom initiation¹¹ applied to this region. This hypothesis is easier to test and more precise than
60 the critical depth hypothesis¹² because the surface mixed-layer is not always associated with
61 strong rates of turbulent mixing^{1,24}. As a second step, we investigated the hypothesis that
62 subseasonal modulations in vertical stability triggered by wind bursts (and reflected by temporal
63 variations in NHF) explain subseasonal SChl variations during the initial states of the bloom in
64 the Northwestern Mediterranean Sea. The paper ends with a discussion on uncertainties and
65 wider implications of these results.

66

67 **Results**

68 Our focus is on the winter (January-February) to spring (March-April) period, which
69 covers the entire SChl bloom from its onset to its decay. This is also when storms are the most
70 frequent and subseasonal variations in SChl are intense⁸. We first describe the main seasonal
71 changes in SChl between winter and spring and relate them to changes in NHF. We then extend
72 the analysis to subseasonal fluctuations.

73 The Northwestern Mediterranean Sea is one of the few regions in the world's ocean
74 where deep convection occurs²⁵. During winter, a deep-mixed patch of dense, nutrient rich water
75 is formed during intense mixing episodes and appears as a blue zone devoid of SChl in ocean
76 color images²⁶ (Fig. 1a). The air-sea heat budget shows a mean seasonal trend from strong
77 buoyancy losses in winter to strong gains in spring, associated with warming. This trend drives

78 seasonal stratification. Consequently, in spring, the pattern in SChl is the reverse figure of the
79 winter pattern (Fig. 1b): the largest spring SChl values mirror the lowest SChl winter values,
80 which delineate the convective area and the corresponding largest winter nutrient inputs²⁷.

81 SChl time series between winter and spring in the core of the bloom region between 2008
82 and 2016 provide a few examples of the annually repeating SChl spring bloom (GOL Box, Fig.
83 2). The complete time series from 1998-2017 is provided in Supplementary Fig. S1. SChl are
84 generally lowest in February, increase sharply around mid-March and decrease in April. There
85 are numerous exceptions to this general rule, and these will be discussed later. For now, we
86 examine whether the main seasonal increase in SChl occurs concurrently with the change of sign
87 in NHF, in support of the convection shut down hypothesis¹¹.

88 A general feature is that the NHF turns positive in mid-March and remains positive
89 thereafter (Fig. 2 and Supplementary Fig. S1). This change of sign consistently coincides with a
90 sharp increase in SChl. This is more quantitatively seen in Figure 3a which shows the value of
91 the SChl net growth rate at the time at which NHF turns and remains positive ($t=0$) and at three
92 consecutive 8-day periods before and after $t=0$ ($t=-24d, -16d, -8d, 8d, 16d, 24d$), over the entire
93 time series (1998-2017) and for the entire bloom region. Averaged over all events, the net
94 growth rate is $\sim 0.1 \text{ day}^{-1}$ at $t=0$ but it is close to zero otherwise. Indeed, the net growth rate is
95 always strictly positive (between 0 and 0.2 day^{-1}) for each individual event at $t=0$, whereas
96 before and after $t=0$, net growth rates are more equally distributed between positive and negative
97 values. This result expands the results of Ferrari et al.¹¹ to the Northwestern Mediterranean Sea.
98 Incidentally, Figure 3a also reveals large values of the standard deviation of the net growth rates,
99 indicating large values of the net growth rate at times before and after $t=0$, which we will
100 examine thereafter.

101 Now we examine the subseasonal events that punctuate the mean seasonal evolution.
102 These subseasonal variations have large intensity both during winter and during spring, although
103 the spatial extent of the region where their intensity is large is more limited in winter than in
104 spring (Fig. 1c,d). Subseasonal variations induce a large variety of typologies of the SChl
105 evolution (Fig. 2 and Supplementary Fig. S1). The seasonal evolution of SChl seldom shows as a
106 single period of rapid SChl accumulation in spring. There can be early periods of accumulation
107 in February (2008, 2011), a series of two to three well separated periods of accumulation of

108 similar magnitude during spring (2008, 2015), a main period of accumulation followed by (2010,
109 2012) or preceded by (2011, 2014) smaller peaks, or double-headed peaks (2009, 2013, 2016).

110 In order to explore the link between short term episodes of calm weather in winter or
111 intensified mixing in spring with intraseasonal SChl fluctuations, we examined the relationship
112 between the time derivative of the NHF and the net SChl growth rate, for each 8-day time step in
113 winter and spring. The underlying assumption is that periods of reduced mixing during winter
114 should correspond to less negative NHF (and lower wind stress), while periods of intensified
115 mixing in spring correspond to lower NHF (and stronger wind stress). The comparison of NHF
116 and wind stress (WS) time series (Fig. 2 and Supplementary Fig. S1) clearly reveals that
117 subseasonal variations of NHF mirror those of the WS. One recurrent feature is that the seasonal
118 increase in NHF is interrupted by storms that last for about one time step (i.e. less than a week).
119 These storms occur several times every year and some were particularly strong such as in Feb
120 2012. Some winters were rather mild (2008, 2014, 2016), some springs particularly stormy
121 (2008, 2009, 2015). Over the bloom region, and from 1998 to 2017, the relative proportion of 8-
122 day bins during which a positive variation in NHF (or a negative variation in WS) was associated
123 with a positive variation in SChl or vice-versa was around 70% in winter and 55% in spring (Fig.
124 1e-f).

125 We examined separately three types of situations which we distinguished based on the
126 sign of the NHF during two consecutive 8-day time steps (Fig. 3b-d): (1) the unstable winter
127 situation, when active turbulent mixing takes place (NHF are negative during the first 8-day time
128 step and remain negative during the following time step), (2) the transition phase, when
129 convection shuts down (NHF are negative during the first time step and positive during the
130 second time step) or when convection resumes (NHF are positive during the first time step and
131 switch to negative during the second time step) and (3) the stable spring situation, when mixing
132 is weak (NHF are initially positive and remain positive). There were several years (for instance
133 2008, 2010 and 2013) where the NHF oscillated between positive and negative values before
134 transitioning to positive. During such years, in Figure 3a, we only accounted for the last zero-
135 crossing to test the convection shutdown hypothesis, as in Ferrari et al.¹¹. In Figure 3b, which
136 shows the net growth rate against the time derivative of the NHF during the transition period, we
137 accounted for all zero-crossing events. This enabled us to extend the initial concept of the

138 convection shutdown hypothesis to weekly fluctuations. We recall that by definition, during the
139 transition period, the NHF at two consecutive time steps have opposed signs. Thus by
140 construction in Figure 3b, positive zero-crossings are on the right quadrant (i.e. NHF switches
141 from negative to positive indicating a positive time derivative) and negative zero-crossing on the
142 left quadrant of the panel (i.e. NHF switches from positive to negative corresponding to a
143 negative time derivative). An important result for the transition period is that positive zero-
144 crossings are always associated with positive net growth rates, showing that the convection
145 shutdown hypothesis not only applies to the main period of net positive growth (last zero-
146 crossing from negative to positive), but also to all subseasonal events that occur before the NHF
147 definitely turns positive. In addition, negative zero-crossings are associated with negative net
148 growth rates and the strength of the net SChl growth is, to a large extent, proportional to the time
149 derivative in NHF (more specifically to changes in latent and sensible heat flux, Supplementary
150 Fig. S2). Because of the strong correlation (~ -0.8) between weekly changes in NHF and WS
151 (Fig. 2), a similar relationship is found when using the rate of change in wind stress
152 (Supplementary Fig. S2). With our initial assumption that during winter and early spring, the rate
153 of change in NHF measures the change in vertical stability, these results show that during the
154 onset phase of the bloom, subseasonal fluctuations in SChl are driven by the intermittency in
155 vertical stability: when NHF decrease, vertical stability decreases and SChl decreases, and vice
156 versa. A similar relationship is found during the unstable winter situation, with net positive
157 growth when NHF increase and net negative growth when NHF decrease (Fig. 3c and
158 Supplementary Fig. S2). We can note that in winter the slope is flatter, illustrating that changes
159 in vertical stability have a weaker impact on the net growth rate when the background situation is
160 already strongly unstable. In contrast, during the mature phase of the bloom (Fig. 3d),
161 fluctuations in net SChl growth rates are only connected to negative changes in NHF; unlike
162 during more unstable periods, a positive change in NHF which causes even more stratification is
163 not associated with net growth. Another interesting difference is that the NHF derivative and the
164 net growth rates remarkably cross at the 0.0 point in winter and transition periods, but not in
165 spring. This indicates that net growth is close to zero in winter and early spring in the absence of
166 significant variations in atmospheric forcing, but in spring it is on average negative
167 independently of the external atmospheric forcing. This is suggestive that mechanisms internal to
168 the ecosystem (such as grazing) exert a significant control on SChl in spring.

169 **Discussion**

170

171 The Northwestern Mediterranean Sea bloom shares many characteristics with the North
172 Atlantic spring bloom²¹, with the particularity that its spatial extension is constrained to the area
173 of winter deep convection, in the center of the cyclonic circulation of the Ligurian Sea (Fig. 1).
174 Early modelling studies of the water column²⁸ and subsequent in-situ observations^{23,6} have
175 suggested that, as for the North Atlantic, the seasonal accumulation in SChl resulted from the
176 alleviation of light limitation on phytoplankton growth, triggered by the reduction in vertical
177 mixing associated with the cessation of deep convection. In light of these earlier studies, we
178 revisited the link between vertical stability and phytoplankton accumulation using two decades
179 of ocean color data confronted to two decades of atmospheric reanalysis. Our results support the
180 convection shut down hypothesis¹⁰ which states that the seasonal surface bloom is initiated by
181 the shut down of vertical mixing induced by the seasonal change of sign in the NHF. We should
182 note that this hypothesis does not seem to apply universally to all bloom regions of the world's
183 ocean. It was clearly demonstrated in the North Atlantic^{11,18} but was less convincing in the North
184 Pacific and Southern Ocean²⁹. Other studies have reported that a reduction in wind speed may
185 also lead to a drop in turbulent mixing and cause the bloom onset, for instance around New
186 Zealand and in the Irminger Basin^{30,16}.

187

188 The seasonal paradigm explains the variability in the timing of bloom initiation, which is
189 well constrained by the time at which the net heat flux switches from negative to positive and
190 remains positive. But it is not sufficient to explain the strong year-to-year variability in bloom
191 phenology. Here we argue that an overlooked complexity is that the bloom of the Northwestern
192 Mediterranean Sea is largely chaotic in response to the chaotic nature of wind bursts (the so-
193 called Mistral and Tramontane) occurring in winter and spring. In winter, the violent mixing
194 episodes leading to deep convection generally last for less than a week, and can occur several
195 times during the same winter with periods of calm weather in between^{31,32,26}. During early
196 spring, strong winds associated to large heat losses are able to destabilize the newly and weakly
197 stratified water column. These storms lead to strong intermittency in vertical stability. We
198 demonstrated that weekly intermittency in both NHF and WS were in phase with the chaotic
199 fluctuations of SChl during periods of low vertical stability. When the NHF was negative or

200 close to zero and the wind intermittently reduced, increases in NHF were associated with
201 increases in SChl; when the wind increased, reductions in NHF were associated with reductions
202 in SChl (Fig. 3). It is out of the scope of this study to precisely characterize the link between the
203 intensity of vertical mixing and the changes in NHF and WS. Nevertheless our results suggest
204 that changes in NHF and wind may be rapidly translated into changes in vertical mixing
205 intensity, affecting light exposure of phytoplankton and their accumulation rates.

206
207 We found a large spread in the relationship between our indexes of vertical stability and
208 phytoplankton net growth rates (Supplementary Fig. S2). This spread questions our hypothesis
209 that phytoplankton net growth rate depends essentially on vertical stability. Other factors, such as
210 variability in phytoplankton loss rates, come into play and may cause some deviation. Another
211 reason is that, in addition to the atmospheric forcing, vertical stability can be affected by the
212 (sub-)mesoscale circulation³³. Particularly in this region of deep water formation, it has been
213 shown that eddies, which participate in the restratification following deep convection, impact
214 deep convection³⁴⁻³⁵, the spring phytoplankton bloom^{28,36} and can cause the bloom to start prior
215 to seasonal stratification³⁷. In the North Atlantic subpolar gyre, Lacour et al.⁹ observed transient
216 winter blooms from autonomous bio-optical profiling floats that they attributed to intermittent
217 restratification by mixed-layer eddies. The 8-day resolution of the satellite SChl hinders our
218 ability to detect shifts of less than 8 days, nevertheless there were some years, like 2008, 2011
219 and 2014, where the increase in SChl was clearly ahead of time compared with the change of
220 sign in NHF, supporting the hypothesis of intermittent eddy-driven stratification. Nevertheless,
221 the strong connection between changes in net growth rates and changes in atmospheric
222 conditions evidenced in this study (about 70% of the time in winter Fig. 1e) suggests that
223 cessation of wind bursts plays a leading order role on driving winter bloom compared with
224 purely oceanic eddy processes in this region.

225
226 During the mature phase of the bloom in April (Fig. 3d), phytoplankton net growth rates
227 continued varying with large subseasonal variations, but with less systematic connections with
228 atmospheric forcing. During this period of more steady physical conditions, other processes
229 such as top down control or nutrient limitation come into play, and the phytoplankton phenology
230 moves from a physical control to a stronger biological control. It is possible that subseasonal

231 variations during this period ensue from intrinsic variability related to biological interactions,
232 due for instance to predator-prey interactions³⁸, or competition of different phytoplankton species
233 for resources^{39,21}.

234
235 We should note that previous studies that have explored the link between storminess and
236 subseasonal fluctuations in phytoplankton were focussed on summer stable conditions, during
237 which phytoplankton growth is limited by nutrient availability rather than light⁴⁰⁻⁴⁴. In that case,
238 storms tend to favor productivity by supplying nutrients to the otherwise depleted euphotic layer.
239 The situation explored here shows an opposite relationship: storms are associated with reduced
240 SChl. Two cases of weekly fluctuations emerge from our analysis. The first is the case of
241 intermittent cessation of harsh atmospheric conditions, which allows the development of short
242 blooms during periods of temporary alleviated light limitation (upper right quadrants in Fig. 3b-c,
243 positive net growth and positive NHF derivative). The second is the case of storms that
244 temporarily interrupts phytoplankton accumulation, with net growth at the surface decreasing in
245 response to the dilution of phytoplankton by vertical mixing (lower left quadrants in Fig. 3b-c-d,
246 negative net growth and negative NHF derivative).

247
248 It is important to highlight that our analysis is based on surface chlorophyll data, and that
249 a distinction is to be made between the surface chlorophyll signal and the vertically integrated
250 phytoplankton carbon biomass. The former is easy to routinely monitor through remote sensing
251 and is characterized by a sharp increase in early spring when conditions become favorable. The
252 latter is only accessible through costly and disparate in-situ observations collected from various
253 observing means^{45,46,7} and can show an increase that starts before the surface bloom and at a
254 slower rate when the integrated phytoplankton population growth rate and loss rate are
255 decoupled^{46,47,7}. In the case of subseasonal SChl fluctuations, one may wonder whether they
256 reflect variations in total biomass, variations in carbon to chlorophyll ratios or essentially mirror
257 dilution when the vertical extent of mixing varies. The field experiment carried out from July
258 2012 to July 2013 in the Gulf of Lion (GOL box in Figure 1) provides some insight to these
259 questions⁶. During the 2013 winter-spring transition, variations in particulate organic matter in
260 the mixed-layer were monitored, and mirrored those of SChl. This observation, even if limited in
261 time, suggests that subseasonal SChl variations can be interpreted as variations in surface carbon

262 biomass in winter and spring. Also, interestingly, the 2013 bloom was interrupted by a strong
263 wind event in mid-March (Fig. 2). Temporal vertical profiles of chlorophyll observed during that
264 event⁶ unambiguously showed that the drop in SChl was solely due to dilution of chlorophyll
265 well below the euphotic layer. Nevertheless a lagged effect (by approximately one week) with
266 increased integrated chlorophyll was also observed, suggesting the possibility of more complex
267 net growth dynamics for total biomass, which may result from reduced grazing due to dilution⁴⁷
268 following the wind event.

269
270 An open question is the overall importance of subseasonal events on the functioning of
271 the system. Our analysis suggests that the brief and episodic variations in phytoplankton
272 observed during the transition from winter to spring ensue from variations in vertical stability
273 that modulate phytoplankton growth rates. These variations are likely to shape the composition
274 of the entire plankton community. For instance, Lacour et al.⁹ reported a community shift from
275 pico and nanophytoplankton to diatoms during transient winter blooms, that likely trigger a
276 similar shift in zooplankton species. A recent analysis based on profiling float measurements in
277 the North Atlantic also revealed short-term changes in grazing during the spring bloom
278 transition⁷. These different manners by which subseasonal variations in vertical stability affect
279 herbivores predation and therefore growth, are likely to influence the transfer of energy to the
280 higher trophic levels⁴⁸.

281
282 Finally, our results suggest that subseasonal events potentially make a significant
283 contribution to the annual export of carbon to the ocean's interior. First, because the community
284 shift to larger phytoplankton species should be associated with large export through the
285 gravitational pump⁹. Second, because intermittent storms during the bloom trigger export through
286 dilution⁶, through the so-called mixed-layer pump⁵⁰. Our results show that these strong events of
287 mixed-layer pump export can be identified with adequate time-series of SChl and NHF, but
288 vertical data would be needed to quantify the quantity of organic material being exported. Given
289 the prevalence of SChl subseasonal events during the bloom and the important role they might
290 have on export production and food web dynamics, more dedicated studies are needed to
291 improve our understanding of these events and their consequences.

292

293 **Data and Methods**

294 We analysed concomitant time series of SChl and atmospheric reanalysis (NHF and WS)
295 over the period 1998-2017 in the bloom region of the Northwestern Mediterranean sea (delimited
296 by the black contour in Fig. 1). For SChl, we used the 8-day, 4 km x 4 km resolution, level 3
297 mapped ocean color product (release 3.1) distributed by the European Space Agency Ocean
298 Color Climate Change Initiative (ESA OC-CCI) available at <http://www.oceancolour.org/>. Each
299 time step represents the averaged SChl value over a period of eight days, estimated from all
300 available daily ocean color observations during the time period. This 8-day product has excellent
301 data coverage in the Northwestern Mediterranean Sea⁸. We used WS and air-sea NHF from the
302 ECMWF ERA Interim reanalysis⁴⁹ available at daily and 0.125° x 0.125° spatial resolution from
303 <https://apps.ecmwf.int/datasets/data/interim-full-daily/>. NHF were computed as the sum of the
304 shortwave radiation, long wave radiation, latent heat flux and sensible heat flux. WS was
305 computed from zonal and meridional surface wind components. In order to facilitate comparison
306 between data sets, atmospheric data were averaged over the 8-day temporal grid of SChl and
307 SChl data were interpolated over the spatial atmospheric grid. Our statistics are thus based on the
308 comparison of SChl, NHF and WS time-series at each pixel in the bloom region, with a 8-day
309 time resolution and 0.125° spatial resolution (a total of 394 pixels and 305 time steps for the
310 bloom region over 1998-2017).

311 Vertical stability is decreased during storms in response to the mechanical action of the
312 wind and to the loss in buoyancy that goes with it. We used time derivatives of WS and NHF as
313 a proxy for intermittent changes in vertical stability. Strong positive changes in WS ($d(WS)/dt$
314 >0 , corresponding to $d(NHF)/dt <0$) indicated the passage of storms, while negative changes in
315 WS ($d(WS)/dt <0$, corresponding to $d(NHF)/dt >0$) marked the return to low wind conditions. In
316 this study, results are shown using $d(NHF)/dt$; the corresponding analysis using $d(WS)/dt$ is
317 provided in the supplementary material.

318 Phytoplankton net growth rates (in units of day^{-1}) are computed as the time derivative of
319 SChl in log scale, $d(\ln(\text{SChl})/dt)$. All time derivatives (Net growth, WS, NHF) are computed
320 between two consecutive 8-day time steps.

321 All the figures in this manuscript are generated using SAXO
322 (<http://forge.ipsl.jussieu.fr/saxo/download/xmldoc/whatissaxo.html>) based on IDL-6.4
323 (Interactive Data Language).

324

325 **References**

- 326 1. Franks, P. J. Has Sverdrup's critical depth hypothesis been tested? Mixed layers vs. turbulent
327 layers. *ICES J. Mar. Sci.*, **72**, 1897-1907, (2015).
- 328 2. Thomalla, S. J., Fauchereau, N., Swart, S., & Monteiro, P. M. S. Regional scale
329 characteristics of the seasonal cycle of chlorophyll in the Southern Ocean. *Biogeosciences*, **8**,
330 2849-2866, (2011).
- 331 3. Thomalla, S. J., Racault, M. F., Swart, S., & Monteiro, P. M. High-resolution view of the
332 spring bloom initiation and net community production in the Subantarctic Southern Ocean
333 using glider data. *ICES J. Mar. Sci.*, **72**, 1999-2020, (2015).
- 334 4. Vantrepotte, V., & Mélin, F. Inter-annual variations in the SeaWiFS global chlorophyll a
335 concentration (1997–2007). *Deep Sea Res. Part I: Oceanogr. Res. Pap.*, **58**, 429-441, (2011).
- 336 5. Salgado-Hernanz, P. M., Racault, M. F., Font-Muñoz, J. S., & Basterretxea, G. Trends in
337 phytoplankton phenology in the Mediterranean Sea based on ocean-colour remote sensing.
338 *Remote Sens. Environ.*, **221**, 50-64, (2019).
- 339 6. Mayot, N. et al. Physical and biogeochemical controls of the phytoplankton blooms in North
340 Western Mediterranean Sea: A multiplatform approach over a complete annual cycle (2012–
341 2013 DEWEX experiment). *J. Geophys. Res. Oceans*, **122**, 9999-10019, (2017).
- 342 7. Yang, B. et al. Phytoplankton Phenology in the North Atlantic: Insights From Profiling Float
343 Measurements. *Front. Mar. Sci.*, **7**, 139, (2020).
- 344 8. Keerthi, M. G., Levy, M., Aumont, O., Lengaigne, M., & Antoine, D. Contrasted
345 Contribution of Intraseasonal Time Scales to Surface Chlorophyll Variations in a Bloom and
346 an Oligotrophic Regime. *J. Geophys. Res. Oceans*, **125**, e2019JC015701, (2020).
- 347 9. Lacour, L., Ardyna, M., Stec, K.F., Claustre, H., Prieur, L., Poteau, A., D'Alcala, M.R., &
348 Ludicone, D. Unexpected winter phytoplankton blooms in the North Atlantic subpolar gyre.
349 *Nat. Geosci.*, **10**, 836-839, (2017).

- 350 10. Taylor, J. R., & Ferrari, R. Shutdown of turbulent convection as a new criterion for the onset
351 of spring phytoplankton blooms. *Limnol. Oceanogr.*, **56**, 2293-2307, (2011).
- 352 11. Ferrari, R., Merrifield, S. T., & Taylor, J. R. Shutdown of convection triggers increase of
353 surface chlorophyll. *J. Marine Syst.*, **147**, 116-122, (2015).
- 354 12. Sverdrup, H. U. On conditions for the vernal blooming of phytoplankton. *J. Cons. Int.*
355 *Explor. Mer.*, **18**, 287-295, (1953).
- 356 13. Huisman, J. E. F., van Oostveen, P., & Weissing, F. J. Critical depth and critical turbulence:
357 two different mechanisms for the development of phytoplankton blooms. *Limnol. Oceanogr.*,
358 **44**, 1781-1787, (1999).
- 359 14. Huisman, J., Arrayás, M., Ebert, U., & Sommeijer, B. How do sinking phytoplankton species
360 manage to persist?. *Am. Nat.*, **159**, 245-254, (2002).
- 361 15. Huisman, J., Sharples, J., Stroom, J. M., Visser, P. M., Kardinaal, W. E. A., Verspagen, J.
362 M., & Sommeijer, B. Changes in turbulent mixing shift competition for light between
363 phytoplankton species. *Ecology*, **85**, 2960-2970, (2004).
- 364 16. Chiswell, S. M., Bradford-Grieve, J., Hadfield, M. G., & Kennan, S. C. Climatology of
365 surface chlorophyll a, autumn - winter and spring blooms in the southwest Pacific Ocean. *J.*
366 *Geophys. Res. Oceans*, **118**, 1003-1018, (2013).
- 367 17. Brody, S. R., & Lozier, M. S. Changes in dominant mixing length scales as a driver of
368 subpolar phytoplankton bloom initiation in the North Atlantic. *Geophys. Res. Lett.*, **41**, 3197-
369 3203, (2014).
- 370 18. Brody, S. R., & Lozier, M. S. Characterizing upper-ocean mixing and its effect on the spring
371 phytoplankton bloom with in situ data. *ICES J. Mar. Sci.*, **72**, 1961-1970, (2015).
- 372 19. Platt, T., Fuentes-Yaco, C., & Frank, K. T. Spring algal bloom and larval fish survival.
373 *Nature*, **423**, 398-399, (2003).
- 374 20. Lutz, M. J., Caldeira, K., Dunbar, R. B., & Behrenfeld, M. J. Seasonal rhythms of net
375 primary production and particulate organic carbon flux to depth describe the efficiency of
376 biological pump in the global ocean. *J. Geophys. Res. Oceans*, **112**, (2007).
- 377 21. Mayot, N., Nival, P. and Levy, M. Primary Production in the Ligurian Sea. *The*
378 *Mediterranean Sea in the Era of Global Change 1: 30 Years of Multidisciplinary Study of the*
379 *Ligurian Sea*, 139-164, (2020).

- 380 22. d'Ortenzio, F., & Ribera d'Alcalà, M. On the trophic regimes of the Mediterranean Sea: a
381 satellite analysis. *Biogeosciences*, **6**, 139-148, (2009).
- 382 23. Lavigne, H. et al. Enhancing the comprehension of mixed layer depth control on the
383 Mediterranean phytoplankton phenology. *J. Geophys. Res. Oceans*, **118**, 3416-3430, (2013).
- 384 24. Carranza, M. M., Gille, S. T., Franks, P. J., Johnson, K. S., Pinkel, R., & Girton, J. B. When
385 mixed layers are not mixed. Storm-driven mixing and bio-optical vertical gradients in
386 mixed layers of the Southern Ocean. *J. Geophys. Res. Oceans*, **123**, 7264-7289, (2018).
- 387 25. Herrmann, M., Somot, S., Sevault, F., Estournel, C., & Déqué, M. Modeling the deep
388 convection in the northwestern Mediterranean Sea using an eddy-permitting and an eddy-
389 resolving model: Case study of winter 1986–1987. *J. Geophys. Res. Oceans*, **113**, (2008).
- 390 26. Testor, P. et al. Multiscale observations of deep convection in the northwestern
391 Mediterranean Sea during winter 2012–2013 using multiple platforms. *J. Geophys. Res.*
392 *Oceans*, **123**, 1745-1776, (2018).
- 393 27. Herrmann, M., Diaz, F., Estournel, C., Marsaleix, P., & Ulses, C. Impact of atmospheric and
394 oceanic interannual variability on the Northwestern Mediterranean Sea pelagic planktonic
395 ecosystem and associated carbon cycle. *J. Geophys. Res. Oceans*, **118**, 5792-5813, (2013).
- 396 28. Levy, M., Memery, L., & Madec, G. The onset of a bloom after deep winter convection in
397 the northwestern Mediterranean sea: mesoscale process study with a primitive equation
398 model. *J. Marine Syst*, **16**, 7-21, (1998).
- 399 29. Cole, H. S., Henson, S., Martin, A. P., & Yool, A. Basin-wide mechanisms for spring bloom
400 initiation: how typical is the North Atlantic?. *ICES J. Mar. Sci*, **72**, 2029-2040, (2015).
- 401 30. Henson, S. A., Robinson, I., Allen, J. T., & Waniek, J. J. Effect of meteorological conditions
402 on interannual variability in timing and magnitude of the spring bloom in the Irminger Basin,
403 North Atlantic. *Deep Sea Res. Part I: Oceanogr. Res. Pap*, **53**, 1601-1615, (2006).
- 404 31. Houpert, L. et al. Observations of open-ocean deep convection in the northwestern M
405 editerranean S ea: Seasonal and interannual variability of mixing and deep water masses for
406 the 2007-2013 Period. *J. Geophys. Res. Oceans*, **121**, 8139-8171, (2016).
- 407 32. Waldman, R. et al. Modeling the intense 2012–2013 dense water formation event in the
408 northwestern Mediterranean Sea: Evaluation with an ensemble simulation approach. *J.*
409 *Geophys. Res. Oceans*, **122**, 1297-1324, (2017a).

- 410 33. Mahadevan, A., D'Asaro, E., Lee, C., & Perry, M. J. Eddy-driven stratification initiates
411 North Atlantic spring phytoplankton blooms. *Science*, **337**, 54-58, (2012).
- 412 34. Waldman, R. et al. Impact of the Mesoscale Dynamics on Ocean Deep Convection: The
413 2012-2013 Case Study in the Northwestern Mediterranean Sea. *J. Geophys. Res. Oceans*,
414 **122**, 8813–8840, (2017b).
- 415 35. Bosse, A. et al. Scales and dynamics of Submesoscale Coherent Vortices formed by deep
416 convection in the northwestern Mediterranean Sea. *J. Geophys. Res. Oceans*, **121**, 7716-
417 7742, (2016).
- 418 36. Lévy, M., Mémery, L., & Madec, G. The onset of the spring bloom in the MEDOC area:
419 mesoscale spatial variability. *Deep Sea Res. Part I: Oceanogr. Res. Pap*, **46**, 1137-1160,
420 (1999).
- 421 37. Lévy, M., Mémery, L., & Madec, G. Combined effects of mesoscale processes and
422 atmospheric high-frequency variability on the spring bloom in the MEDOC area. *Deep Sea*
423 *Res. Part I: Oceanogr. Res. Pap*, **47**, 27-53, (2000).
- 424 38. Fussmann, G. F., Ellner, S. P., Shertzer, K. W., & Hairston Jr, N. G. Crossing the Hopf
425 bifurcation in a live predator-prey system. *Science*, **290**, 1358-1360, (2000).
- 426 39. Huisman, J., & Weissing, F. J. Fundamental unpredictability in multispecies competition.
427 *Am. Nat.*, **157**, 488-494, (2001).
- 428 40. Fauchereau, N., Tagliabue, A., Bopp, L., & Monteiro, P. M. The response of phytoplankton
429 biomass to transient mixing events in the Southern Ocean. *Geophys. Res. Lett*, **38**, (2011).
- 430 41. Carranza, M. M., & Gille, S. T. (2015). Southern Ocean wind - driven entrainment enhances
431 satellite chlorophyll - a through the summer. *J. Geophys. Res. Oceans*, **120**, 304-323.
- 432 42. Menkès, C. E. et al. Global impact of tropical cyclones on primary production. *Global*
433 *Biogeochem. Cy.*, **30**, 767-786, (2016).
- 434 43. Nicholson, S. A., Lévy, M., Jouanno, J., Capet, X., Swart, S., & Monteiro, P. M. S. Iron
435 supply pathways between the surface and subsurface waters of the Southern Ocean: from
436 winter entrainment to summer storms. *Geophys. Res. Lett*, **46**, 14567-14575, (2019).
- 437 44. Nicholson, S. A., Lévy, M., Llort, J., Swart, S., & Monteiro, P. M. Investigation into the
438 impact of storms on sustaining summer primary productivity in the Sub - Antarctic Ocean.
439 *Geophys. Res. Lett*, **43**, 9192-9199, (2016).

- 440 45. Boss, E., & Behrenfeld, M. In situ evaluation of the initiation of the North Atlantic
441 phytoplankton bloom. *Geophys. Res. Lett.*, **37**, (2010).
- 442 46. Mignot, A., Ferrari, R., & Claustre, H. Floats with bio-optical sensors reveal what processes
443 trigger the North Atlantic bloom. *Nat. commun.*, **9**, 1-9, (2018).
- 444 47. Behrenfeld, M. J. Abandoning Sverdrup's critical depth hypothesis on phytoplankton blooms.
445 *Ecology*, **91**, 977-989, (2010).
- 446 48. Mitra, A. et al. Bridging the gap between marine biogeochemical and fisheries sciences;
447 configuring the zooplankton link. *Prog. Oceanogr.*, **129**, 176-199, (2014).
- 448 49. Dee, D. P. et al. The ERA - Interim reanalysis: Configuration and performance of the data
449 assimilation system. *Q. J. Roy. Meteor Soc.*, **137**, 553-597, (2011).
- 450 50. Boyd, P. W., Claustre, H., Levy, M., Siegel, D. A., & Weber, T. Multi-faceted particle
451 pumps drive carbon sequestration in the ocean. *Nature*, 568(7752), 1–9, (2019).
- 452

453 **Acknowledgments**

454 The authors acknowledge the support from CNES (Centre National d'Etudes Spatiales) and
455 ANR-SOBUMS (Agence Nationale de la Recherche, contract number : ANR-16-CE01-0014) for
456 this research. Keerthi M G is supported by a postdoctoral fellowship from CNES.

457

458

459 **Author contribution**

460 MGK, ML and OA conceived and developed the study. MGK performed the data analysis and
461 made the plots. ML, MGK and OA made the interpretation of the results. ML and MGK wrote
462 the manuscript and OA reviewed it. ML and OA supervised the whole research.

463

464

465

466 **Additional Information**

467

468 **Competing interests statement** : The authors declare no competing interests.

469 **Figure Legends**

470

471 **Figure 1: (a-b)** Surface Chlorophyll climatology (SChl, in mgChl.m^{-3}) in the Northwestern
472 Mediterranean Sea in winter (January-February) and spring (March-April), over the period 1998-
473 2017. **(c-d)** Standard deviation (STD) of intraseasonal SChl fluctuations (SChl-ISV) in winter
474 (resp. spring), normalized by the mean SChl in winter (resp. spring). Intraseasonal SChl
475 fluctuations were extracted from the total signal using the Census X-11 technique, following
476 Keerthi et al.⁸. **(e-f)** Percentage of time steps for which the time derivative in Net Heat Flux and
477 the SChl net growth rate have the same sign, during winter and during spring. In all panels, the
478 black contour delimitates the bloom region, which we defined as the region where the
479 climatological spring SChl is greater than $0.65 \text{ mg.}(\text{Chl}).\text{m}^{-3}$. The black square marks the Gulf of
480 Lion (GOL) box.

481

482 **Figure 2:** Timeseries of Surface Chlorophyll (SChl, green curves), Net Heat Flux (NHF, red
483 curves) and wind stress (blue curves) averaged over the GOL box between January and May,
484 from 2008 to 2016. The pink shading highlights the spring period (March-April).

485

486 **Figure 3:** SChl net growth rate (in day^{-1}) **(a-b)** during the **winter to spring transition phase:**
487 when the NHF changes sign, **(c)** during the **unstable winter phase:** when NHF are initially
488 negative and remain negative and **(d)** during the **stable spring phase:** when NHF is initially
489 positive and remains positive. **(a)** SChl net growth rate is shown against time (in days) since the
490 NHF has switched from negative to positive and has remained positive thereafter ($t_{\text{NHF}}=0$).
491 The mean net growth at $t=0$ is larger than at any time step before ($t=-24\text{d}, -16\text{d}, -8\text{d}$) or after
492 ($t=8\text{d}, 16\text{d}, 24\text{d}$). **(b-d)** SChl net growth rate against temporal changes in NHF. Positive (resp.
493 negative) changes in NHF are used as a proxy for increased (resp. decreased) vertical stability. In
494 winter and early spring, increased (resp. decreased) vertical stability at weekly time scale are
495 associated with enhanced (resp. decreased) net growth rate. SChl Growth rates are computed for
496 individual events, i.e. at each 8-day time step and at each $0.125^\circ \times 0.125^\circ$ pixel in the bloom
497 region over 1998-2017 within the time period January-April, and are then bin-averaged, with the
498 vertical bars representing one standard deviation. Data of each single event before bin-averaging
499 are shown in Supplementary Figure S2.

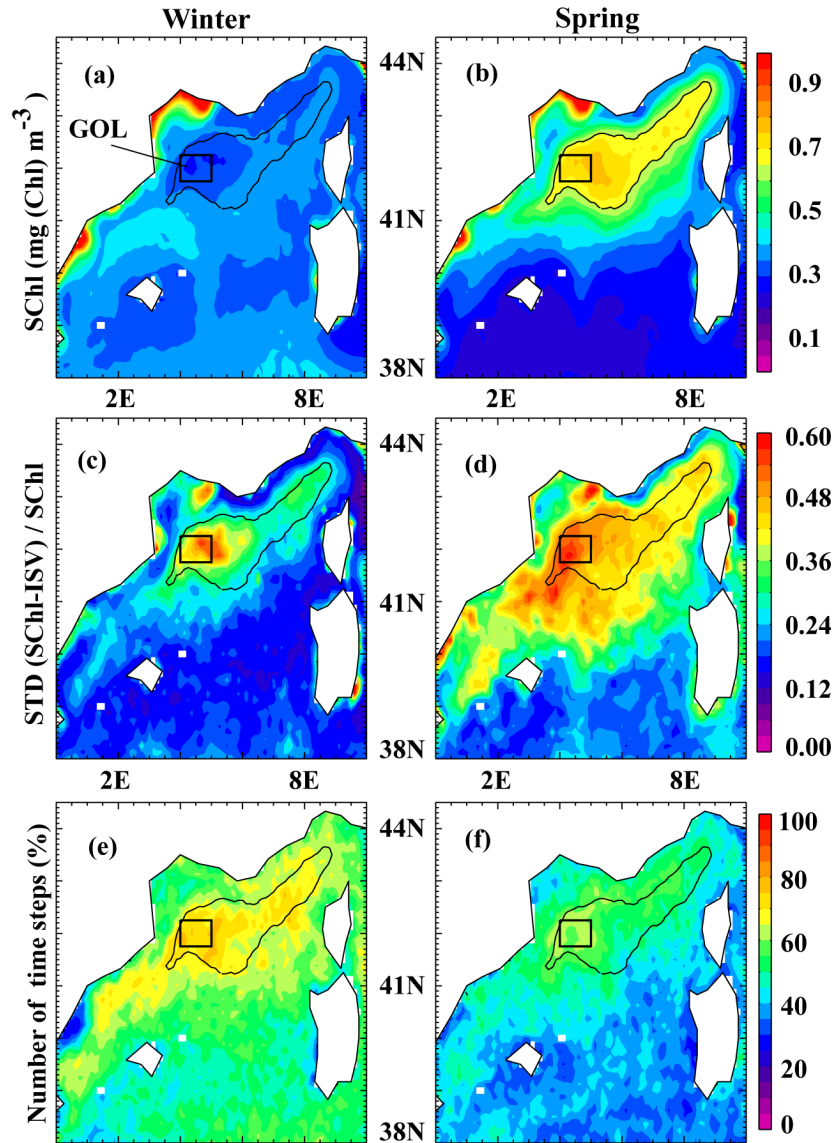


Figure 1: (a-b) Surface Chlorophyll climatology (SChl, in $\text{mgChl}\cdot\text{m}^{-3}$) in the Northwestern Mediterranean Sea in winter (January-February) and spring (March-April), over the period 1998-2017. (c-d) Standard deviation (STD) of intraseasonal SChl fluctuations (SChl-ISV) in winter (resp. spring), normalized by the mean SChl in winter (resp. spring). Intraseasonal SChl fluctuations were extracted from the total signal using the Census X-11 technique, following Keerthi et al.⁸. (e-f) Percentage of time steps for which the time derivative in Net Heat Flux and the SChl net growth rate have the same sign, during winter and during spring. In all panels, the black contour delimitates the bloom region, which we defined as the region where the climatological spring SChl is greater than $0.65 \text{ mg}\cdot(\text{Chl})\cdot\text{m}^{-3}$. The black square marks the Gulf of Lion (GOL) box.

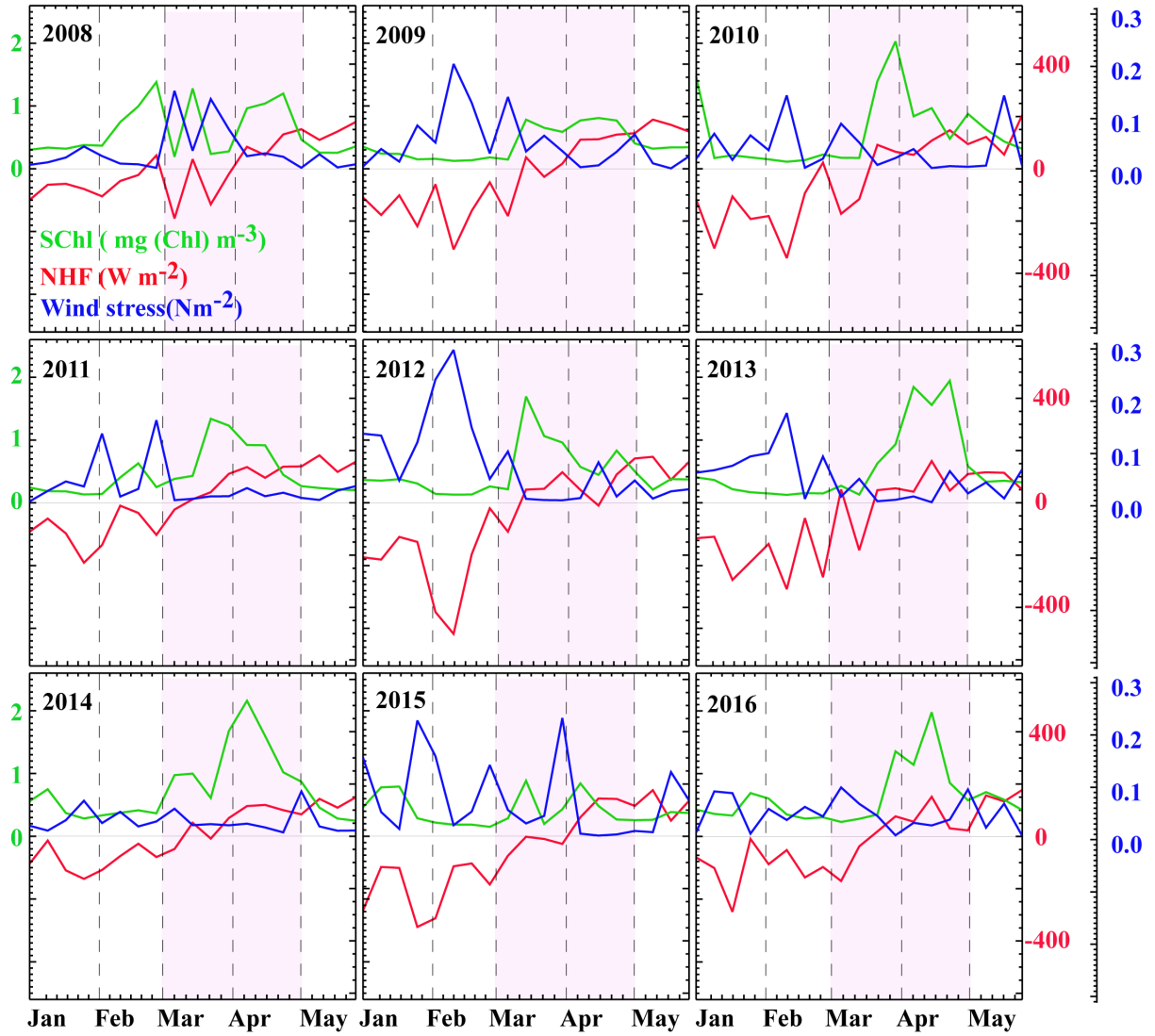


Figure 2: Timeseries of Surface Chlorophyll (SChl, green curves), Net Heat Flux (NHF, red curves) and wind stress (blue curves) averaged over the GOL box between January and May, from 2008 to 2016. The pink shading highlights the spring period (March-April).

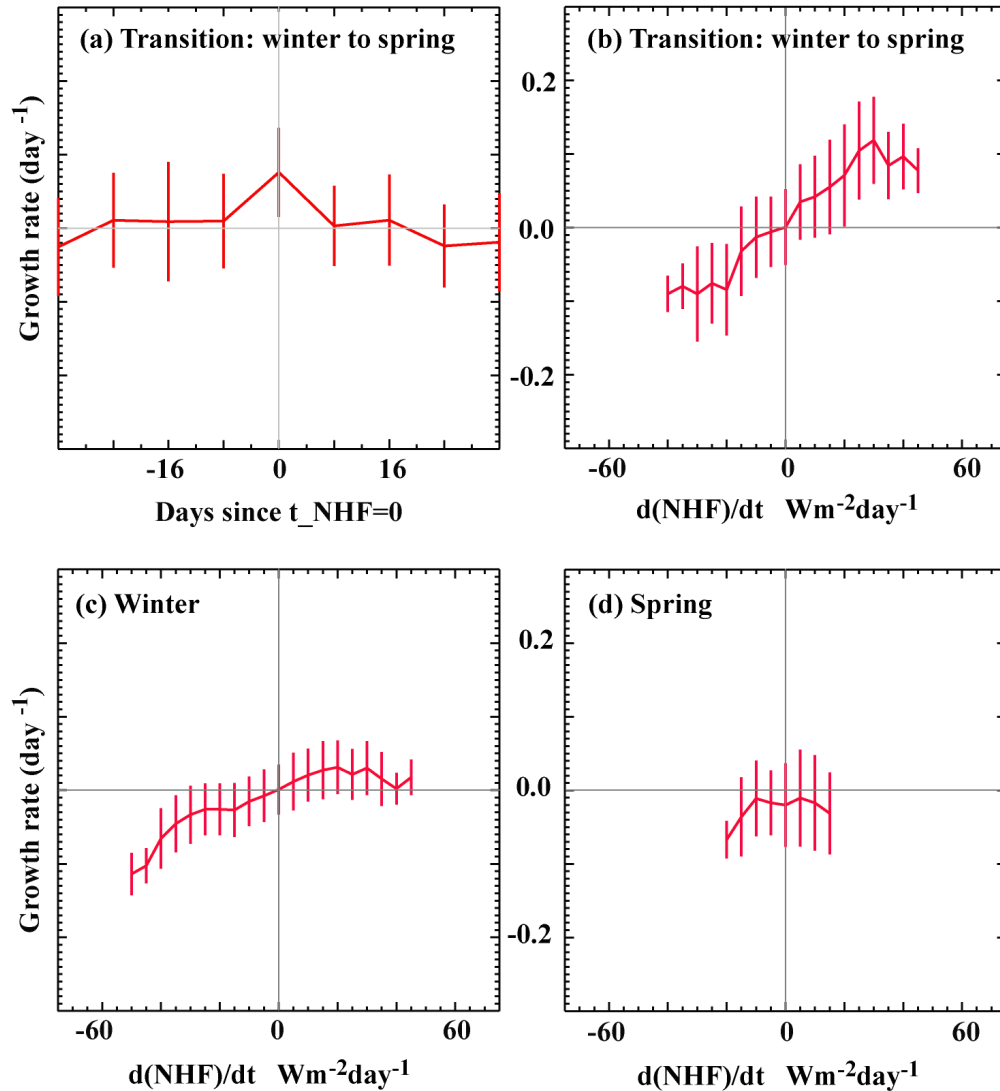


Figure 3: SCHl net growth rate (in day^{-1}) **(a-b)** during the **winter to spring transition phase**: when the NHF changes sign, **(c)** during the **unstable winter phase**: when NHF are initially negative and remain negative and **(d)** during **the stable spring phase**: when NHF is initially positive and remains positive. **(a)** SCHl net growth rate is shown against time (in days) since the NHF has switched from negative to positive and has remained positive thereafter ($t_{\text{NHF}}=0$). The mean net growth at $t=0$ is larger than at any time step before ($t=-24\text{d}$, -16d , -8d) or after ($t=8\text{d}$, 16d , 24d). **(b-d)** SCHl net growth rate against temporal changes in NHF. Positive (resp. negative) changes in NHF are used as a proxy for increased (resp. decreased) vertical stability. In winter and early spring, increased (resp. decreased) vertical stability at weekly time scale are associated with enhanced (resp. decreased) net growth rate. SCHl Growth rates are computed for individual events, i.e. at each 8-day time step and at each $0.125^\circ \times 0.125^\circ$ pixel in the bloom region over 1998-2017 within the time period January-April, and are then bin-averaged, with the vertical bars representing one standard deviation. Data of each single event before bin-averaging are shown in Supplementary Figure S2.